Excitation and charge transfer in proton-hydrogen collisions

A. Kołakowska, M. S. Pindzola, and F. Robicheaux

Department of Physics, Auburn University, Auburn, Alabama 36849

D. R. Schultz

Physics Division, Oak Ridge National Laboratory, Oak Ridge, Tennessee 37831

J. C. Wells

Center for Computational Sciences, Oak Ridge National Laboratory, Oak Ridge, Tennessee 37831

Excitation and charge transfer cross sections for collisions of protons with hydrogen are calculated by direct solution of the time-dependent Schrödinger equation on a three-dimensional Cartesian lattice. The $2s$, $2p$, $3s$, $3p$, and $3d$ excitation cross sections and the $1s$, $2s$, $2p$, $3s$, $3p$, and $3d$ charge transfer cross sections from the $1s$ ground state at 10-, 40-, and 100-keV incident proton energy are found by projecting a time-evolved wave function onto the lattice target states of hydrogen. Excitation processes are calculated in the rest frame of the hydrogen atom, while capture processes are calculated in the rest frame of the proton. The computed excitation and charge transfer cross sections are in good agreement with recent experiments and other theoretical results based on coupled-channels methods. [S1050-2947(98)03210-7]

PACS number(s): 34.70.+e

I. INTRODUCTION

The proton-hydrogen collision remains a benchmark for the development of new atomic scattering theories. There are three basic inelastic processes that take place: excitation of the target, electron capture by the projectile, and direct ionization. Despite the basic nature of this three-body collision, there are still discrepancies between theory and experiment, and differences among the results of various theoretical approaches. On the experimental side, proton-hydrogen collisions have been studied extensively, and at present there is a large number of experimental cross sections for excitation [1–4] and charge transfer [5–15] over a wide energy range. On the computational side, there is no general approach that gives accurate inelastic cross sections at all energies. At high collision energies the Born approximation does well, but it does not predict the correct energy dependence for the inelastic cross sections at lower energies. For electron excitation and capture processes at intermediate impact energies, close-coupling [16–19] and distorted wave [20–22] methods have been widely applied. Although quite successful, the close-coupling methods may run into basis state convergence difficulties [17,18] when extended over too great an energy range.

An additional theoretical approach for ion-atom collisions is the direct solution of the time-dependent Schrödinger (or Hartree-Fock) equation on a numerical lattice [23–27]. Due to the long-range nature of the Coulomb electrostatic force, however, only the substantial advances in computer technology realized over the last few years have allowed the possibility of carrying out full three-dimensional lattice solutions. Recently, a 3D lattice solution has been successfully employed to study the excitation and ionization of hydrogenic atoms by collisions with antiprotons [28–30]. In this paper we attempt a 3D lattice solution of the time-dependent Schrödinger equation for proton-impact excitation of and charge transfer with the neutral hydrogen atom. A general advantage of the lattice method lies in its application over a wide energy range. A numerical lattice method makes no assumption regarding the suitability of any particular basis set expansion. A further advantage is that collision dynamics may be easily visualized since the total wave function is calculated explicitly as a function of time. Our 3D lattice solution of the time-dependent Schrödinger equation is carried out in Cartesian coordinates. A straight-line classical trajectory for the proton across the lattice may then be characterized with a single impact parameter. We consider two alternative numerical methods: (1) low-order finite differences using a staggered leapfrog propagator and (2) Fourier collocation using a split-operator propagator. The first method was chosen because of its straightforward implementation on distributed-memory parallel computers. The second method was chosen because the total wave function may be represented to the same accuracy on a relatively more sparse grid. Lattice size is generally the main determinant of overall computational time. In both numerical methods, observables are obtained by projecting the total wave function following the collision onto the stationary states of the system. Excitation processes are studied in the rest frame of the hydrogen atom target, while capture processes are studied in the rest frame of the proton projectile. The computational lattice methods are outlined in Sec. II, the results for excitation and charge transfer to the $n = 1, 2, 3$ shells are presented and discussed in Sec. III, and a brief summary is found in Sec. IV. Atomic units are used throughout unless otherwise noted.

II. THEORY

The time-dependent Schrödinger equation for a bare ion (Z_p) projectile colliding on a classical trajectory with a hy-

drogenic atom (Z_t) target is given by

$$i \frac{\partial \Psi(\vec{r},t)}{\partial t} = \left(-\frac{1}{2}\nabla^2 - \frac{Z_t}{r} - \frac{Z_p}{R(t)} \right) \Psi(\vec{r},t), \qquad (1)$$

where $\vec{r}$ is the electron position vector with respect to the target and $R(t)$ is the time-dependent distance between the projectile and target. The above equation may also be used to describe a hydrogenic atom projectile colliding with a bare ion target. We solve Eq. (1) with the boundary conditions described below using two different lattice techniques to obtain a discrete representation of the wave function and all operators on a three-dimensional Cartesian coordinate grid.

A. Finite-difference method

For easy implementation on distributed-memory parallel computers, second-order finite-difference methods are employed with uniform mesh spacing. For example, the kinetic energy has a lattice representation in terms of a tridiagonal matrix, while the electron-ion interaction operator is a diagonal matrix. For straight-line motion in the y direction,

$$R(t) = \sqrt{(x-b)^2 + [y-(y_0+vt)]^2 + z^2}, \qquad (2)$$

where y_0 and the impact parameter b locate the initial position of the projectile and v is the projectile velocity. The choice of an xy scattering plane guarantees that the collision Hamiltonian has reflection symmetry with respect to the $z=0$ plane. We divide the lattice into xy planar layers and propagate the wave function for each layer on a separate processor. Solution of the Schrödinger equation only involves nearest surface layer message passing. Due to the $z=0$ plane reflection symmetry, the layers only extend from $z=0$ to $z=z_{max}$ with the additional condition of $\Psi(x,y,0,t) = 0$ for $\Psi(\vec{r},0)$ equal to an initial function that is odd in z, and $\partial\Psi(x,y,0,t)/\partial z = 0$ for $\Psi(\vec{r},0)$ equal to an initial function that is even in z.

The eigenfunctions, $\psi_n(\vec{r})$, and eigenenergies, E_n, for the ground and low-lying excited states of the hydrogenic atom may be found by propagating the Schrödinger equation in imaginary time ($\tau=it$) [31]:

$$\psi_n(\vec{r},\tau+\Delta\tau) = e^{-H_0\Delta\tau}\psi_n(\vec{r},\tau), \qquad (3)$$

where

$$H_0 = -\frac{1}{2}\nabla^2 - \frac{Z_t}{r}. \qquad (4)$$

Since $\Delta\tau$ is inversely related to the maximum energy, E_{max}, on the lattice, we may also use an iterative relaxation in energy:

$$\psi_n^{i+1}(\vec{r}) = \prod_{k=1}^{N} \left(\frac{k}{N}E_{max} - H_0 \right) \psi_n^i(\vec{r}). \qquad (5)$$

In practice we have found that $N=4$ works quite well, starting from the analytic wave functions for a hydrogenic atom. Schmidt orthogonalization in every iteration prevents collapse of excited states to lower-energy states of the same

symmetry. The termination criterion is based on the energy differences obtained in two consecutive iterations. In practice the method rapidly converges in just a few iterations.

With the initial condition $\Psi(\vec{r},t=0) = \psi_{1s}(\vec{r})$, the time-dependent Schrödinger equation was propagated in real time using an explicit "staggered leapfrog" algorithm [32]. The method is ideal for distributed-memory parallel computers since it involves only simple matrix-vector multiplication at each time step. Spurious wave reflection at the lattice boundary is eliminated through the use of exponential masking. In one coordinate the masking function has the form

$$F_{mask}(x) = 1 - e^{-\xi(x_{max}-x)} - e^{+\xi(x_{min}-x)}, \qquad (6)$$

where ξ is a suitable positive constant that depends on the lattice extent. At each step in the time propagation the wave function is multiplied by a mask function for each coordinate. We note that the mask function in the z coordinate does not contain the exponential term with $z_{min}=0$.

To calculate excitation cross sections we center the hydrogenic wave function, $\psi_{1s}(\vec{r})$, at the origin of the coordinate system and let the bare ion move across the lattice. The probability of excitation to a $\psi_{n\ell m}(\vec{r})$ state for a given projectile velocity and impact parameter is given by

$$P_{n\ell m}(v,b) = \left| \int d^3r\, \psi_{n\ell m}^*(\vec{r})\Psi(\vec{r},t=T) \right|^2, \qquad (7)$$

where T is the time when the projectile reaches the lattice boundary. The $1s \rightarrow n\ell m$ excitation cross section for a given projectile velocity is given by

$$\sigma_{n\ell m}(v) = 2\pi \int_0^\infty db\, b\, P_{n\ell m}(v,b). \qquad (8)$$

Due to the reflection symmetry through the $z=0$ plane, we need only consider final states with the same $(-1)^{\ell+m}$ reflection number as the initial state (i.e., even r number for the $1s$ state). To calculate charge transfer cross sections we center the translated hydrogenic wave function, $\psi_{1s}(\vec{r})e^{ivy}$, at $\vec{r}=(b,y_0,0)$ and let the hydrogenic atom move across the lattice. The capture probabilities and cross sections are calculated as before using Eqs. (7) and (8).

B. Fourier collocation method

The Fourier-collocation method for the time-dependent Schrödinger equation describing ion-atom collisions with a single active electron has been previously discussed in detail [29]. The reader is referred to this paper for a description of the strengths and weaknesses of our implementation of this numerical approach. An advantage of such high-order methods is an improved numerical representation of the high-energy part of the energy-momentum dispersion relationship [33]. This characteristic often results in fewer lattice points being required for a solution with specified accuracy as compared to low-order methods, assuming the solutions are sufficiently smooth. The lattice parameters used in performing the calculations presented in this work are identical to those used before [29] (i.e., 135^3 lattice points in a cubic numerical

TABLE I. Hydrogen atom solutions on a finite-difference lattice. For each nlm state, the first row contains results obtained on the grid that includes zero, while the second row list results obtained with no zero on the grid.

State	$\langle H_0 \rangle$	$\langle r \rangle$	$\left\langle \dfrac{1}{r} \right\rangle$	$2\langle T \rangle + \langle V \rangle$	$\sqrt{\langle H_0 \rangle^2 - \langle H_0^2 \rangle}$
$1s_0$	-0.49999	1.49	0.97	$+7.3 \times 10^{-3}$	3.2×10^{-4}
	-0.49515	1.51	0.98	-8.9×10^{-3}	2.3×10^{-4}
$2s_0$	-0.12525	5.99	0.25	$+9.1 \times 10^{-4}$	3.6×10^{-4}
	-0.12457	6.00	0.25	-2.1×10^{-4}	3.7×10^{-4}
$2p_{+1}$	-0.12505	4.99	0.25	-1.9×10^{-4}	9.3×10^{-4}
	-0.12514	4.99	0.25	-2.8×10^{-4}	2.0×10^{-3}
$2p_{-1}$	-0.12505	4.99	0.25	-1.9×10^{-4}	9.3×10^{-4}
	-0.12514	4.99	0.25	-2.8×10^{-4}	2.0×10^{-3}
$3s_0$	-0.05562	13.47	0.11	$+6.0 \times 10^{-4}$	4.1×10^{-4}
	-0.05541	13.48	0.11	-1.0×10^{-4}	4.1×10^{-4}
$3p_{+1}$	-0.05557	12.48	0.11	$+1.2 \times 10^{-4}$	2.8×10^{-4}
	-0.05559	12.48	0.11	$+1.8 \times 10^{-4}$	3.1×10^{-4}
$3p_{-1}$	-0.05557	12.48	0.11	$+1.2 \times 10^{-4}$	2.8×10^{-4}
	-0.05559	12.48	0.11	$+1.8 \times 10^{-4}$	3.1×10^{-4}
$3d_0$	-0.05556	10.49	0.11	$+3.8 \times 10^{-5}$	2.3×10^{-4}
	-0.05557	10.49	0.11	$+3.8 \times 10^{-5}$	2.3×10^{-4}
$3d_{+2}$	-0.05556	10.49	0.11	$+9.3 \times 10^{-6}$	2.6×10^{-4}
	-0.05557	10.49	0.11	$+1.0 \times 10^{-5}$	2.7×10^{-4}
$3d_{-2}$	-0.05556	10.49	0.11	$+9.3 \times 10^{-6}$	2.6×10^{-4}
	-0.05557	10.49	0.11	$+1.0 \times 10^{-5}$	2.7×10^{-4}

box of length 52 a.u. with a complex potential absorbing outgoing flux near the edges of the box). Use of an efficient split-operator method of time propagation in the present work has also resulted in a significant decrease in computational effort over our previous work using a Taylor series expansion of the time propagator. We note that the Fourier-collocation method is implemented via fast Fourier transforms. As a result of this choice, we do not take advantage of the symmetry with respect to the collision plane as is discussed regarding the present finite-differences method. Implementation of this approach on shared-memory parallel computers is straightforward, since good parallel fast-Fourier transform software routines are available.

III. RESULTS AND DISCUSSION

Excitation and charge transfer cross sections from the $1s$ ground state of hydrogen at 10-, 40-, and 100-keV incident proton energy are calculated by the direct solution of the time-dependent Schrödinger equation on a three-dimensional Cartesian lattice. The finite difference calculations use a lattice of $300 \times 300 \times 150$ points with a uniform grid spacing of $\Delta x = \Delta y = \Delta z = 0.2$. Thus the lattice extends from -30 to $+30$ in the x and y directions, and from 0 to $+30$ in the z direction. The Fourier collocation calculations use a lattice of $135 \times 135 \times 135$ points with a uniform grid spacing of 0.385. Thus the lattice extends from -26 to $+26$ in the x, y, and z directions. Both the finite difference and Fourier collocation lattices are sufficiently large to support nearly spectroscopic $n = 1,2,3$ orbitals. To cover the $n = 4$ shell will require even larger lattice sizes.

Energies and other observables for the $n = 1,2,3$ hydrogen

atom solutions on the finite difference lattice are presented in Table I, while similar quantities for the Fourier collocation lattice are found in Tables I and II of the paper by Wells *et al.* [29] on antiproton collisions with hydrogen. Due to the adopted z reflection symmetry in the finite difference lattice only the even r-number functions ($1s_0$, $2s_0$, $2p_{\pm1}$, $3s_0$, $3p_{\pm1}$, $3d_0$, $3d_{\pm2}$) need to be calculated for later use in the cross-section projections. The energy expectation $\langle H_0 \rangle$, the radial expectation values $\langle r \rangle$ and $\langle 1/r \rangle$, the virial theorem, and the energy fluctuation can be compared with their exact values ($\langle H_0 \rangle = -Z_t/2n^2$, $\langle r \rangle = [3n^2 - l(l+1)]/2Z_t$, and $\langle 1/r \rangle = Z_t/n^2$) to provide a test of each lattice representation.

Table I presents a comparison between the results obtained on a finite-difference lattice that includes zero and one that does not include zero. In the first case, the Coulomb potential is modified by the introduction of a soft-core potential, $-Z_t/r \rightarrow -Z_t/\sqrt{c + r^2}$, to avoid the singularity at the origin. The adjustable parameter c is set to 4.5035×10^{-3} to yield a ground-state energy close to -0.5 for a lattice spacing of 0.2. In the second case, the singularity is avoided by placing the origin half-way between the lattice spacing for all three coordinates. In each case the iteration process is terminated when two consecutive energies differ by less than 10^{-7}, which usually happens in less than 30 iterations. In general, three or four decimal places in the listed energies can be obtained with less than six iterations. We note that relatively small values of $2\langle T \rangle + \langle V \rangle$, particularly for $3d$ states, do not necessarily mean that the excited part of the spectrum is approximated better than, say, the ground state. While the result of the virial theorem test for the $1s$ state certainly reflects the difficulty of the lattice representation of
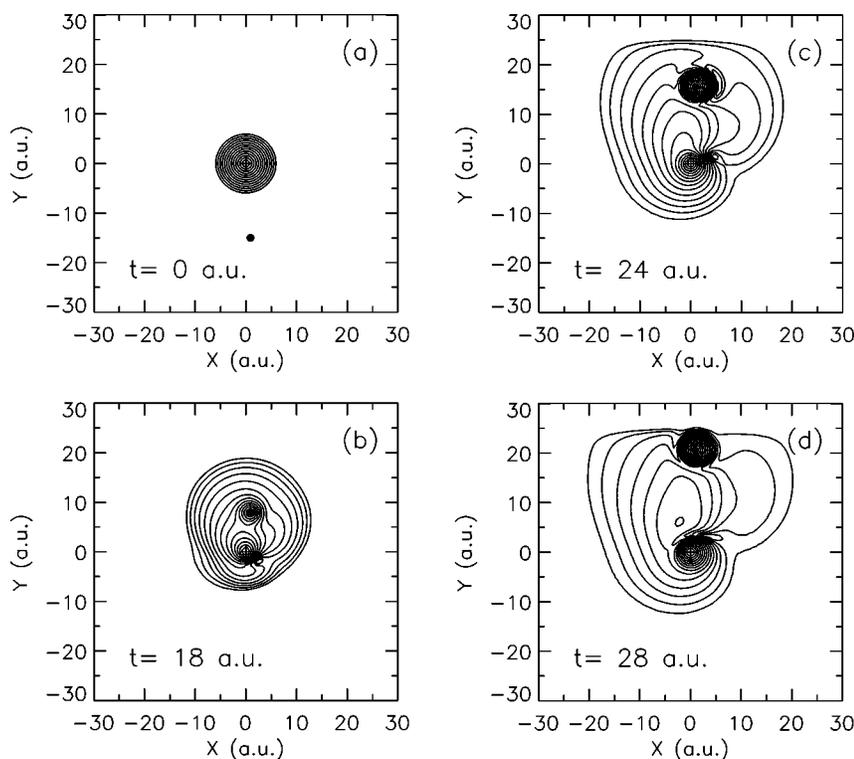
FIG. 1. Excitation: time evolution of the electron density in the $z=0$ scattering plane for an incident proton energy of 40 keV and an impact parameter $b=1.0$.

the Coulomb potential at $r=0$, the $n=3$ numerical orbitals are difficult to determine accurately due to the finite size of the lattice. It is safe to say that while the virial theorem is not exactly valid on the lattice it can still serve as a tool in the evaluation of the computational method; however, care should be taken when it is used to probe the quality of stationary solutions obtained on the lattice. A similar observation is also valid for other expectation values. A comparison of the numerical observables for both cases with the corre-

sponding analytical results shows reasonable agreement. In the finite difference calculations presented in the following paragraphs of this section, we chose the lattice that does not include zero since deviations from exact energy values are less than 1%, and the differences from exact radial expectation values fall below 3%.

We illustrate the visualization power of the lattice method by presenting probability density plots in the $z=0$ scattering plane as a function of time in Figs. 1 and 2 for a proton-
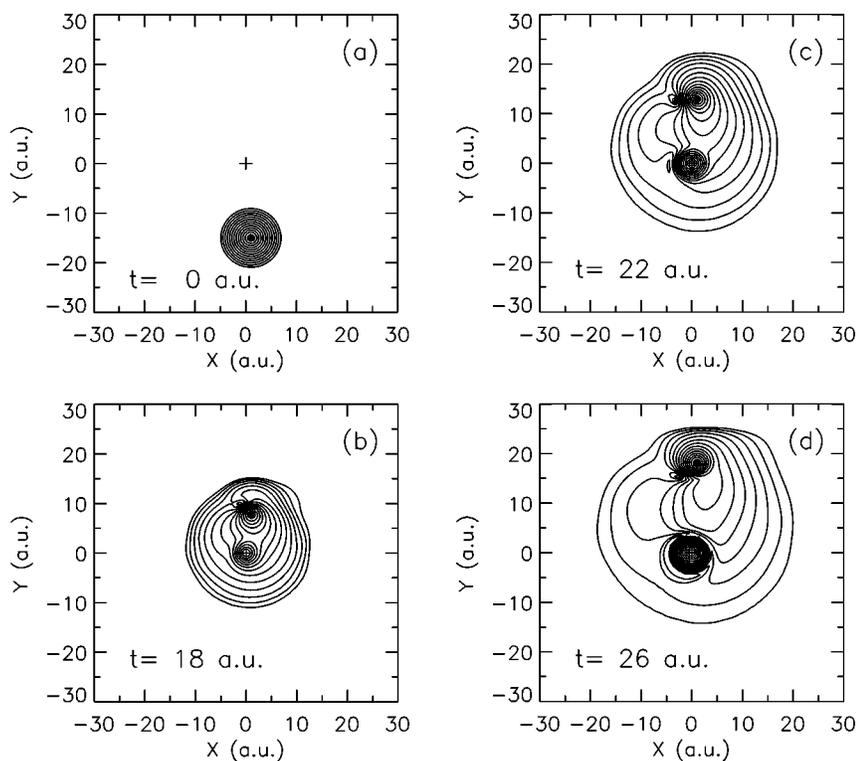
FIG. 2. Charge transfer: time evolution of the electron density in the $z=0$ scattering plane for an incident hydrogen atom energy of 40 keV and an impact parameter $b=1.0$.
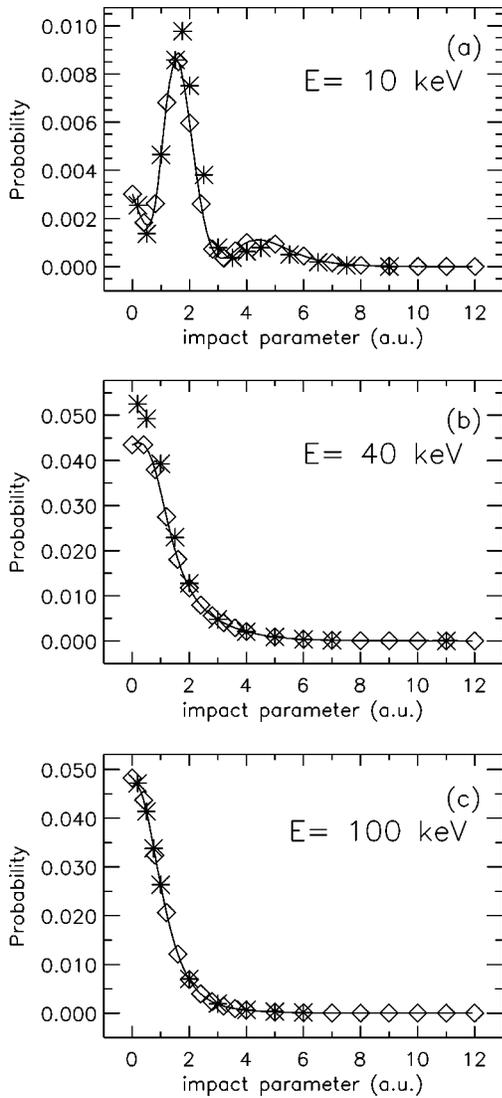
FIG. 3. Probability of excitation to the 2*s* state as a function of impact parameter for selected impact energies: (a) $E=10$ keV, (b) $E=40$ keV, (c) $E=100$ keV. Diamonds are the results from the finite-difference method, asterisks are the results from the Fourier collocation method, and the solid curve is a cubic spline interpolation through the finite-difference results.

FIG. 4. Probability of excitation to the 2*p* state as a function of impact parameter for selected impact energies: (a) $E=10$ keV, (b) $E=40$ keV, (c) $E=100$ keV. Diamonds are the results from the finite-difference method, asterisks are the results from the Fourier collocation method, and the solid curve is a cubic spline interpolation through the finite-difference results.

hydrogen collision at 40 keV. The time propagation of the Schrödinger equation is started for an initial projectile position of $\vec{r}_0=(1.0,-15.0,0.0)$ (an impact parameter $b=1.0$), as depicted in Fig. 1(a) and Fig. 2(a). The time propagation is terminated when the projectile reaches the lattice boundary at $\vec{r}_0=(1.0,+30.0,0.0)$, which is $T=20.0$ for an incident energy of 40 keV. In Fig. 1 the projectile is the proton and the target is the hydrogen atom located at the origin. In Fig. 2 the roles are reversed, the projectile is the hydrogen atom and the target is the proton located at the origin. As mentioned in Sec. II, excitation cross sections can be most easily extracted in the rest frame of the hydrogen atom, while charge transfer cross sections are easily extracted in the rest frame of the proton. An oscillation of the electron density between the projectile and target can be observed in both figures. Another interesting aspect of the two-center collision dynamics is the rotation of electron density about an individual center,

clearly visible in the contour plots. Looking at the final frames in each sequence, i.e., Fig. 1(d) and Fig. 2(d), it can be seen that one is the mirror image of the other, as should be expected, giving a good check on the overall numerical methods.

Excitation in proton-hydrogen collisions is examined using both the finite-difference and Fourier collocation methods. The excitation probabilities [see Eq. (7)] as a function of impact parameter are presented in Fig. 3 for the $1s \rightarrow 2s$ transition and in Fig. 4 for the $1s \rightarrow 2p$ transition at 10-, 40-, and 100-keV incident proton energy. The diamonds are the calculational results from the finite-difference method, the asterisks are the calculational results from the Fourier collocation method, and the solid curve is a cubic spline interpolation of the finite-difference results. As can be seen, there is good agreement between the two lattice methods for the 2*s* and 2*p* excitation probabilities. The overall agreement be-

TABLE II. Excitation cross sections (in units of 10^{-18} cm^2) for proton-hydrogen collisions. Finite-difference method results are labeled (FD), while Fourier collocation method results are labeled (FC).

Final state	Energy (keV)		
	10	40	100
$n=2$	27.2 (FD)	92.3 (FD)	96.1 (FD)
	25.0 (FC)	99.0 (FC)	88.2 (FC)
	26.0 [18]	90.0 [18]	86.0 [18]
		96.40±8.3 [1][a]	91.00[c]±5.5 [1][a]
		88.86±8.3 [1][b]	83.88[c]±5.5 [1][b]
$2s$	5.62 (FD)	16.1 (FD)	9.64 (FD)
	5.54 (FC)	18.2 (FC)	10.1 (FC)
	5.0 [18]	17.0 [18]	10.0 [18]
	5.0±1.5 [8]	17.73[c] [17]	10.2 [17]
	6.1±2.83 [4]	13.9±4.97 [4]	8.7±3.31 [4]
	3.0±0.9 [10]		
$2p$	21.6 (FD)	76.2 (FD)	86.5 (FD)
	19.5 (FC)	80.8 (FC)	78.1 (FC)
	21.2 [18]	71.2 [18]	76.2 [18]
	24.0±1.4 [9]	68.66[c] [17]	76.20 [17]
	25.0±5.0 [8]	62.9±7.548 [3]	82.1±9.852 [3]
	36.0±7.5 [5]		80.0±9.6 [2]
$n=3$	7.25 (FD)	21.0 (FD)	18.2 (FD)
	5.59 (FC)	18.3 (FC)	15.7 (FC)
	7.0 [18]	19.0 [18]	17.0 [18]
		18.14[c] [17]	17.02 [17]
		23.50±2.0 [1][a]	21.75[c]±3.0 [1][a]
		21.66±2.0 [1][b]	20.05[c]±3.0 [1][b]
$3s$	1.04 (FD)	3.51 (FD)	1.96 (FD)
	0.701 (FC)	3.47 (FC)	1.74 (FC)
	0.9 [18]	3.4 [18]	2.1 [18]
		3.94[c] [17]	2.24 [17]
$3p$	3.50 (FD)	12.6 (FD)	14.2 (FD)
	3.22 (FC)	10.6 (FC)	12.3 (FC)
	3.0 [18]	12.0 [18]	13.0 [18]
		10.93[c] [17]	12.92 [17]
		9.5±1.235 [3]	13.7±1.781 [3]
$3d$	2.70 (FD)	4.93 (FD)	2.09 (FD)
	1.67 (FC)	4.25 (FC)	1.62 (FC)
	1.5 [18]	2.75 [18]	1.75 [18]
		3.27[c] [17]	1.86 [17]

[a]Normalized to Born approximation.
[b]Normalized to Glauber approximation.
[c]Value interpolated from published data.

tween the two lattice methods for the $3s$, $3p$, and $3d$ excitation probabilities is also fairly good, with the small discrepancies attributed to the different overall box sizes.

The total excitation cross sections [see Eq. (8)] for intermediate-energy proton-hydrogen collisions calculated with both the finite-difference and Fourier collocation meth-ods are compared with each other, selected alternative theoretical approaches, and available experimental measurements in Table II. The two lattice methods are in reasonable agreement for all transitions at all energies. Comparison is made with the recent single-center expansion coupled states calculation of Ford *et al.* [17] and the two-center atomic orbital
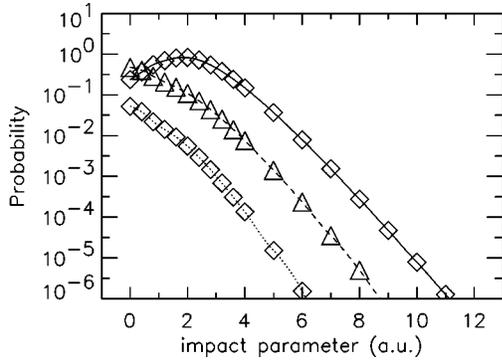
FIG. 5. Probability of charge transfer to the $1s$ state for impact energies 10 keV (solid curve), 40 keV (dashed curve) and 100 keV (dotted curve) as a function of impact parameter.

close-coupling method of Kuang and Lin [18]. For excitation at 40 keV, the single-center expansion method results are linearly interpolated from the reported cross sections at 30 and 45 keV. The lattice calculations are found to be in good agreement with the theoretical predictions of the single-center expansion and two-center atomic orbital methods. Comparison is made with experimental measurements by Park *et al.* [1] of the total excitation cross section to the $n=2$ and $n=3$ shells. For excitation at 100 keV, the experimental cross sections were linearly interpolated from reported measurements at 95 and 105 keV. The experimental cross sections [1] are normalized at 200 keV to theoretical values obtained with either the Born or the Glauber approximations. Both ''normalized'' measurements are included in Table II. The lattice cross sections for $n=2$ and $n=3$ excitation fall within the error bars of the experiment at all energies. Comparison is made with a number of experimental measurements [2–5,8–10] of the total excitation cross section to the $2s$, $2p$, and $3s$ subshells. The lattice results are close to or fall within the error bars for all the measurements, except for the $2s$ cross section at 10 keV reported by Chong and Fite [10] and the $2p$ cross section at 10 keV reported by Stebbings *et al.* [5].

Charge transfer in proton-hydrogen collisions is examined using only the finite-difference method. The capture probabilities as a function of impact parameter are presented in Fig. 5 for the $1s \rightarrow 1s$ transition and in Fig. 6 for both the $1s \rightarrow 2s$ and $1s \rightarrow 2p$ transitions at 10-, 40-, and 100-keV incident proton energy. The diamonds and the triangles are the calculational results from the finite-difference method and the solid, dashed, and dotted curves are cubic spline interpolations of the finite-difference results. Since the $1s$ capture probabilities drop rapidly as a function of the impact parameter, they are displayed on a logarithmic scale. The overall functional dependance on the impact parameter remains the same for the $n=2$ and $n=3$ probabilities, with the absolute values being generally one or two orders of magnitude smaller.

The total integrated charge transfer cross sections for intermediate-energy proton-hydrogen collisions calculated with the finite-difference method is compared to other theoretical approaches and experimental measurements in Table III. Comparison is made with the two-center atomic orbital close-coupling method of Kuang and Lin [18], the con-
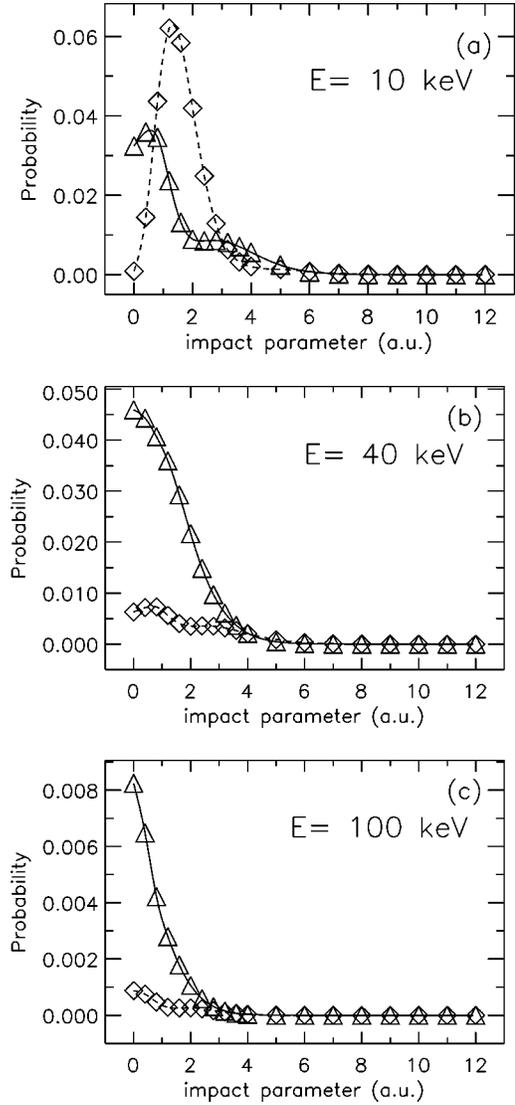
FIG. 6. Probability of charge transfer to the $2s$ (solid curves) and the $2p$ (dashed curves) states as a function of impact parameter for selected impact energies: (a) $E=10$ keV, (b) $E=40$ keV, (c) $E=100$ keV.

tinuum distorted-wave calculations of Belkić *et al.* [20], and the symmetrized variational coupled distorted-wave method of Brown and Crothers [22]. The two-center atomic orbital and symmetrized variational coupled distorted-wave method results are digitized from plots in the original publications. The lattice calculations are found generally to be in good agreement with the other theoretical approaches. The largest discrepancy, by a factor of 3, is with the continuum distorted-wave method for charge transfer to the $3d$ state at 40 keV. Comparison is made with a number of experimental measurements [5–12,14] of the total charge-transfer cross section to the $2s$, $2p$, and $3s$ subshells. The lattice results are close to or fall within the error bars for all the reported measurements.

IV. SUMMARY

By direct solution of the time-dependent Schrödinger equation on a three-dimensional Cartesian lattice, we have

TABLE III. Charge-transfer cross sections (in units of 10^{-18} cm^2) for proton-hydrogen collisions. Only finite-difference method results are presented for comparison.

Final state	Energy (keV)		
	10	40	100
1s	789.0	113.0	6.54
		137.0 [20]	6.39 [20]
		120.0 [18]	8.50 [18]
n=2	53.3	28.2	1.54
		39.40 [20]	1.66 [20]
2s	20.3	21.3	1.26
	24.0 [22]	11.8 [22]	1.00 [22]
	17.8±1.0 [10]	28.1 [20]	1.24 [20]
	26.0±8.0 [8]	25.0 [18]	1.80 [18]
	21.0±6.3 [11]	18.0±1.44 [12]	1.80±0.144 [12]
	24.0±3.0 [7]	20.0±3.0 [7]	1.10±0.3 [6]
2p	33.0	6.94	0.280
	40.0 [22]	5.0 [22]	0.118 [22]
	26.4±1.3 [9]	11.2 [20]	0.291 [20]
	31.0±5.0 [8]	7.0 [18]	0.4 [18]
	38.0±19.0 [5]		
n=3	9.71	9.11	0.500
		13.8 [20]	0.577 [20]
3s	2.60	6.47	0.386
		8.96 [20]	0.402 [20]
		7.0 [18]	0.6 [18]
	4.12±1.06 [14]	6.27±0.40 [14]	0.28±0.09 [14]
3p	3.96	2.24	0.103
		3.85 [20]	0.154 [20]
		1.90 [18]	0.090 [18]
3d	3.14	0.304	0.0107
		1.02 [20]	0.0213 [20]
		0.20 [18]	

calculated excitation and charge-transfer cross sections for proton-hydrogen collisions at intermediate energies. Two different lattice methods have been shown to yield subshell cross sections in good agreement with selected alternative theoretical methods and the available experimental measurements. This study of proton scattering from the hydrogen atom, combined with earlier work on antiproton scattering from hydrogenic atoms [28–30], has demonstrated that the lattice method can be successfully employed to calculate inelastic cross sections for one-electron ion-atom collisions. This success can be attributed in large measure to the substantial advances in computer technology realized over just the last few years. We are currently extending the Fourier collocation method to also handle capture processes and performing further studies on the contribution to excitation and capture from $n > 3$ states. This will allow us to make a reasonable estimate of the total ionization cross section. The challenge in the future is to extend the lattice approach to multiple electron targets through the use of core pseudopotentials and/or time-dependent Hartree-Fock theory. Due to the low symmetry nature of the formulation, the lattice method may also be quite easily adapted to the study of ion-atom collisions in external fields.

[1] J. T. Park, J. E. Aldag, J. M. George, and J. L. Peacher, Phys. Rev. A **14**, 608 (1976).

[2] K.-H. Schartner, D. Detleffsen, and B. Sommer, Phys. Lett. A **136**, 55 (1989).

[3] D. Detleffsen, M. Anton, A. Werner, and K.-H. Schartner, J. Phys. B **27**, 4195 (1994).

[4] D. P. Higgins, J. Geddes, and H. B. Gilbody, J. Phys. B **29**, 1219 (1996).

[5] R. F. Stebbings, R. A. Young, C. L. Oxley, and H. Everhardt, Phys. Rev. **138**, A1312 (1965).

[6] G. Ryding, A. B. Wittkower, and H. B. Gilbody, Proc. Phys. Soc. (London) **89**, 547 (1966).

[7] J. E. Bayfield, Phys. Rev. **185**, 105 (1969).

[8] T. F. Morgan, J. Geddes, and H. B. Gilbody, J. Phys. B **6**, 2118 (1973).

[9] T. Kondow, R. J. Girnius, Y. P. Chang, and W. L. Fite, Phys. Rev. A **10**, 1167 (1974).

[10] Y. P. Chong and W. L. Fite, Phys. Rev. A **16**, 933 (1977).

[11] J. Hill, J. Geddes, and H. B. Gilbody, J. Phys. B **12**, L341 (1979).

[12] T. J. Morgan, J. Stone, and R. Mayo, Phys. Rev. A **22**, 1460 (1980).

[13] H. Tawara, T. Kato, and Y. Nakai, At. Data Nucl. Data Tables **32**, 235 (1985).

[14] M. P. Hughes, J. Geddes, R. W. McCullough, and H. B. Gilbody, Nucl. Instrum. Methods Phys. Res. B **79**, 50 (1993).

[15] H. B Gilbody, Adv. At., Mol., Opt. Phys. **33**, 149 (1994).

[16] W. Fritsch and C. D. Lin, Phys. Rep. **202**, 1 (1991).

[17] A. L. Ford, J. F. Reading, and K. A. Hall, J. Phys. B **26**, 4537 (1993).

[18] J. Kuang and C. D. Lin, J. Phys. B **29**, 5443 (1996); **29**, 1207 (1996).

[19] B. M. McLaughlin, T. G. Winter, and J. F. McCann, J. Phys. B **30**, 1043 (1997).

[20] D. Belkić, R. Gayet, and A. Salin, At. Data Nucl. Data Tables **51**, 59 (1992).

[21] D. S. F. Crothers and L. J. Dube, Adv. At., Mol., Opt. Phys. **30**, 287 (1992).

[22] G. J. N. Brown and D. S. F. Crothers, Phys. Rev. Lett. **76**, 392 (1996).

[23] V. Maruhn-Rezwani, N. Grun, and W. Scheid, Phys. Rev. Lett. **43**, 512 (1979).

[24] C. Bottcher, Phys. Rev. Lett. **48**, 85 (1982).

[25] K. C. Kulander, K. R. Sandhya Devi, and S. E. Koonin, Phys. Rev. A **25**, 2968 (1982).

[26] C. Bottcher, G. J. Bottrell, and M. R. Strayer, Comput. Phys. Commun. **63**, 63 (1991).

[27] N. H. Kwong, K. J. Schaudt, and J. D. Garcia, Comput. Phys. Commun. **63**, 171 (1991).

[28] D. R. Schultz, P. S. Krstic, C. O. Reinhold, and J. C. Wells, Phys. Rev. Lett. **76**, 2882 (1996).

[29] J. C. Wells, D. R. Schultz, P. Gavras, and M. S. Pindzola, Phys. Rev. A **54**, 593 (1996).

[30] D. R. Schultz, J. C. Wells, P. S. Krstic, and C. O. Reinhold, Phys. Rev. A **56**, 3710 (1997).

[31] A. Goldberg and J. L. Schwartz, J. Comput. Phys. **1**, 433 (1967); **1**, 448 (1967).

[32] W. H. Press, S. A. Teukolsky, W. T. Vetterling, and B. P. Flannery, *Numerical Recipes* (Cambridge Press, New York, 1992), p. 833.

[33] J. C. Wells, V. E. Oberacker, M. R. Strayer, and A. S. Umar, Int. J. Mod. Phys. C **6**, 143 (1995).